Electromagnetic Impacts of Interface Discontinuity in Geometry and Material between Tunable and Non-Tunable PCBs for 79 GHz Liquid Crystal Phase Shifters in Joint Communication and Sensing

Jinfeng Li, *Member, IEEE*

Abstract—**Beyond on-wafer measurements that focus exclusively on transmission line characterization, the realization of reconfigurable millimeter-wave (mmW) phase shifters requires the integration of connectors, which introduces the need for electromagnetic (EM) quantification of the interfaces between these connectors and the printed circuit board (PCB)—including both the tunable core line and the non-tunable transition sections. This paper investigates the EM effects of interface discontinuities in hybrid tunable/non-tunable PCB structures for liquid crystal (LC)-based phase shifters operating at 79 GHz for joint communication and sensing (JC&S). Two legacy topologies are examined: Design 1 (symmetric CPW with LC-filled gaps) and Design 2 (partially shielded CPW with integrated top electrodes). The non-tunable PCB sections are deliberately maintained as straight lines—rather than optimized shapes—to isolate material and geometric discontinuity impacts. Full-wave simulations using CST and HFSS are conducted across 1–79 GHz, quantifying S-parameters, surface current density, differential phase shifts, and figure-of-merit (FoM). At 79 GHz, Design 1 achieves a maximum insertion loss of 7.62654 dB at 0 V bias and a maximum phase shift of 408.74755° at 10 V bias, yielding an FoM of 53.59°/dB. Design 2 exhibits 9.64885 dB insertion loss and 347.79376° phase shift, resulting in an FoM of 38.19°/dB. Results demonstrate that interface discontinuities induce higher-order mode propagation and impedance mismatches, significantly affecting performance. The study further assesses the quarter-wavelength transformation approach in multi-interface configurations, revealing deviations from standard 50 Ω impedance strategy. These findings illustrate the importance of rigorous interface characterization for LC-based mmW phase shifters in emerging JC&S applications.**

I. INTRODUCTION

The rising demand for ubiquitous connectivity, propelled by the pervasive integration of the Internet of Everything (IoE) [1–7], has precipitated a rapid advancement in beam-steering device technology across the microwave (MW) [8] and millimeter-wave (mmW) spectra [9]. This frequency upgrade, from legacy bands such as 2.45 GHz toward higher mmW frequencies, is necessitated by the burgeoning requirements for expanded bandwidth capacities as per Shannon's Theorem on data rate [10], which also highlights the significant role of beam-steering in enhancing signal-to-noise ratio.

Within this context, the 79 GHz band [11] has emerged as a particularly compelling frequency for next-generation wireless platforms, as it offers a unique convergence of two critical features: wide contiguous bandwidth (up to 4 GHz) for high-throughput short-range communication, and high range-Doppler resolution for precision sensing. Consequently, 79 GHz is increasingly recognized as a prime candidate for Joint Communication and Sensing (JC&S) systems [12], especially in automotive radar and beyond-5G (B5G) applications, making it an essential frequency for investigating advanced beamforming.

Regarding the technological realization of millimeter-wave (mmW) beam steering, the phased antenna array [9] is arguably a foundational solution that has transitioned from military deployment to commercial applications. At the core of phased array antenna operation, phase modulation [13] serves as the key enabler for subsystem functionality. To address phase reconfigurability, consider the classical two-port transmission line configuration illustrated in Figure 1, characterized by a physical line length L, with the phase at the two ports denoted as Φ_1 and Φ_2, respectively.

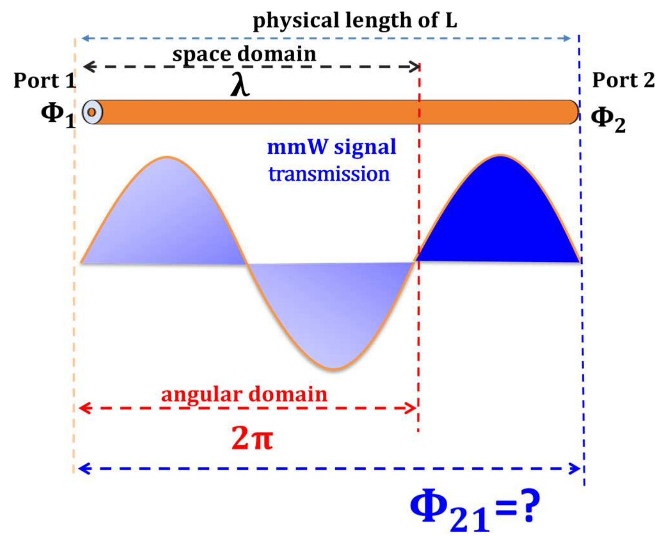

Figure 1. Physical model of a two-port transmission line illustrating phase variation along the line. This model motivates reconsideration of how differential phase shift can be achieved toward a phase shifter.

The angular relationship between the line length L and the effective wavelength λ of the mmW signal propagating within the transmission line is governed by the ratio expressed in (1). Based on this relationship, the output phase referenced to the phase at port 1 can be derived as shown in (2).

*Resrach supported by the National Natural Science Foundation of China.
Jinfeng Li is with Beijing Key Laboratory of Millimeter Wave and Terahertz Technology, Beijing Institute of Technology, Beijing, 100081, China (e-mail: jinfengcambridge@bit.edu.cn).

$$\frac{2\pi}{\Phi_{21}} = \frac{\lambda}{L}, \quad (1)$$

$$\Phi_{21} = \frac{2\pi L}{\lambda}. \quad (2)$$

To enable the phase modulation expressed in (2), two fundamental approaches can be adopted: changing the physical line length L as shown in (3), or varying the effective wavelength λ as shown in (4), wherein c is the speed of light, f is the fixed frequency of operation (i.e., true-time-delay), and ε_{eff} denotes the effective permittivity. Consequently, the technological realizations of these two distinct approaches are based on switches (between transmission lines of varying lengths) and tunable dielectrics (for altering the effective permittivity ε_{eff} and thus the wave propagation velocity), respectively. More specifically, these realizations employ semiconductor switches (e.g., p-i-n diodes [14]) and liquid crystals (LCs) [15], respectively. Differentiating (4) yields the tuning principle equation expressed in (5), which underpins the LC-based reconfigurable phase-shifting approach.

$$\Delta\Phi_{21} = \frac{2\pi\Delta L}{\lambda}. \quad (3)$$

$$\Phi_{21} = \frac{2\pi L}{\lambda} = \frac{2\pi L}{\frac{c}{f\sqrt{\varepsilon_{eff}}}} = \frac{2\pi L\sqrt{\varepsilon_{eff}}}{c} f, \quad (4)$$

$$\Delta\Phi_{21} = \frac{2\pi L(\Delta\sqrt{\varepsilon_{eff}})}{c} f. \quad (5)$$

Concurrently, the escalating demand for flexible, high-performance solutions, coupled with the pursuit of ultra-high temporal and spatial resolution, has catalyzed growing interest in the exploration of LC-based mmW passive components [4][6] for analog modulation of signal phase [16]. This research avenue—continuous tunability of phase manipulation—circumvents the quantization effects [14] inherent in conventional semiconductor switching techniques, which are binary in nature [17].

Empirical evidence has substantiated the dielectric tuning principle [15] and the consequent phase modulation mechanisms [16] of LC-filled phase shifting devices. These devices are constructed from the transmission line principle (as illustrated in Figure 1) and filled with tunable dielectrics (i.e., LC) to perturb the effective wavelength [2]. Readers seeking a comprehensive exploration of LC-based microwave device intricacies are directed to previous studies [18–22], which address device physics [18], chemistry [19], measurement methodologies [20], interpretation of differential phase shift results [21], and application domains [22].

Among the multitude of feasibility assessments of LC-based microwave tunable components, particular emphasis has been placed on the phase shifting functionality of the active core line and its associated insertion loss [18], contingent upon geometric dimensions (the aspect ratio effect [20]) and material dielectric constants [15]. While these endeavors are instrumental in elucidating the underlying physical principles for design purposes, the realization of functional phase shifter devices requires additional considerations, notably interface compatibility with industry-standard connectors. Owing to the liquid-like nature of LC materials, which necessitates their encapsulation within coplanar channels [18] or enclosures [20], material and geometric disparities at interface junctions present significant challenges.

Notably, interface discontinuities—both between LC-filled core line segments and their non-tunable counterparts, and between PCB edges and connector pins—induce higher-order mode propagation, as demonstrated in our prior studies [23] employing time-domain reflectometry (TDR) techniques.

This study extends previous investigations through two case studies employing legacy device topologies (as shown in the cross-sectional geometry sketched at Figure 2). The first topology features an LC-filled symmetric coplanar waveguide (CPW) (see [18] for the design and [24] for experiments) without top floating electrodes. The second topology employs an LC-filled partially enclosed CPW (see [20][25] for design and experiments) with integrated top electrodes connected to the coplanar grounds and an additional LC layer for tuning beneath the metallic enclosure. By incorporating 1.85 mm PCB-mount connectors [26] at the input and output ports, this study aims not to optimize the non-tunable component shapes—a matter addressed in prior work reported in 2020 50th European Microwave Conference (EuMC) [23]—but rather to examine the viability of the classic quarter-wavelength transformation approach [27] in the context of multi-interface configurations, potentially deviating from the standard 50 Ω impedance strategy. Full-wave electromagnetic simulations were conducted using CST Studio Suite and ANSYS HFSS to model and analyze the interface discontinuities across the 1 GHz to 79 GHz frequency range.

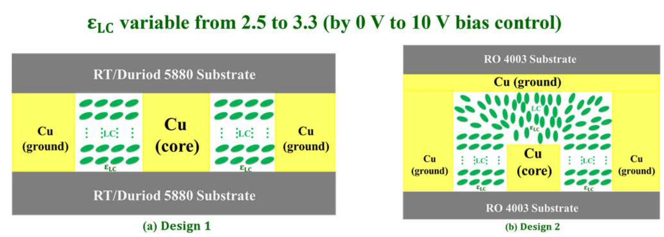

Figure 2. Our two legacy device topologies for LC-accommodated mmW phase shifters with integrated PCB edge-mount connectors: (a) symmetric CPW without top floating electrodes, and (b) partially enclosed CPW with top electrodes electrically and physically connected to coplanar grounds. Nematic LC molecules are illustrated under saturated bias (e.g., 10 V in this study for obtaining the maximally achievable permittivity of 3.3).

II. Discontinuities at Interfaces

A. Underlying Design and Discontinuity Problem Statement

The two designs presented in this study are not intended to be benchmarked against one another in terms of performance. Rather, they serve to provide additional evidence of the interface discontinuity impacts observed in two distinct LC-filled structures: a CPW for Design 1, and a CPW-adapted topology for Design 2. Although the two designs differ substantially in terms of tuning range (per unit length) and loss characteristics, the overarching architecture of the overall device remains broadly similar, as illustrated in Figure 3. The figure depicts multiple reflections along the mmW propagation path; other power flow mechanisms—namely transmission, scattering, and radiation—are not depicted. A side view of the device is presented in Figure 4, while a zoomed-in view of the connector pin interfacing with the PCB (non-tunable dielectric part) is shown in Figure 5 (rendered using CST Studio Suite). The housing (grounding) as well as the core conductors of the connector are modeled as an assembly of discrete arc segments [2]—a simplification inherent to computational models that prioritizes numerical stability and mesh compatibility over faithful representation of the manufactured geometry.

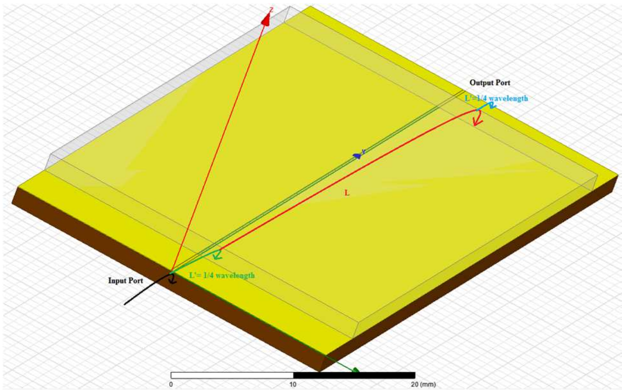

Figure 3. Multiple reflections along the mmW propagation direction from input to output ports of an LC-based CPW-type phase shifter (Design 1).

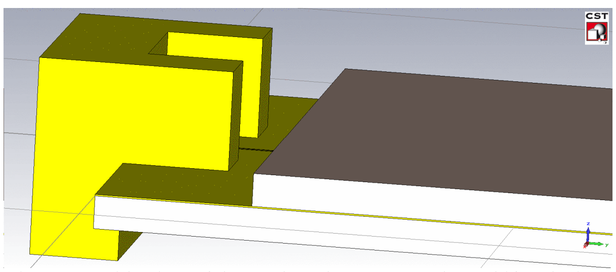

Figure 4. Side view of the LC-based CPW-type phase shifter device.

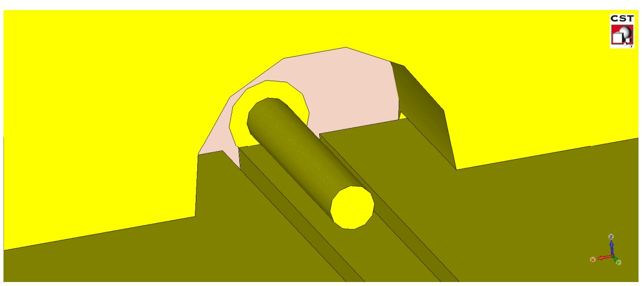

Figure 5. Zoomed-in view of the connector mounted on the edge of device.

B. Two Designs Under Investigation

The objective of this case study is not to optimize the shape of the non-tunable components—a matter previously addressed in [20][23] by proposing an all-50 Ω strategy throughout the transmission line, including the interfaces—but rather to investigate the limitations (or feasibility) of the classic quarter-wavelength transformation approach. In this approach, the length of the dielectrically non-tunable PCB edge sections is selected based on the principle of superposition of reflected waves, thereby permitting non-50 Ω operation when addressing this multi-interface problem.

With regard to the connectors, 9 mil end-launch connectors are used for Design 1, with outer diameter B equal to 9 mil (0.2286 mm) and inner diameter A equal to 5 mil (0.13 mm). For Design 2, 20 mil end-launch connectors are employed. As illustrated in Figure 6, the outer diameter (denoted as B) measures 20 mil (0.508 mm), while the inner diameter (denoted as A) measures 10 mil (0.254 mm).

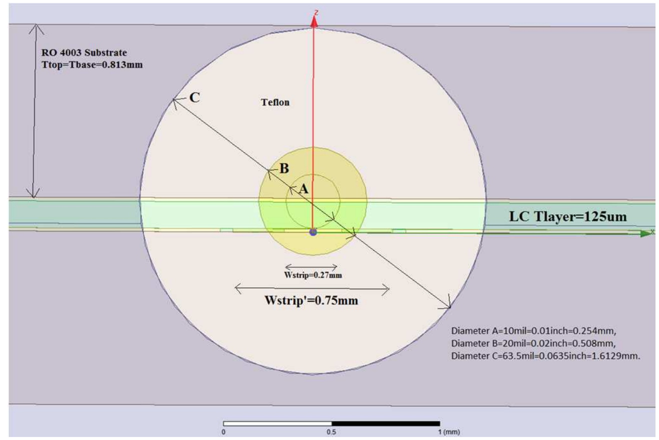

Figure 6. Cross-sectional illustration of 20 mil end-launch connectors mounted on the PCB edge of Design 2.

Regarding the transmission line length, Table I summarizes the dimensions along the mmW propagation path for both designs. The PCB width in both designs is 2.5 cm.

TABLE I. LINE LENGTH DIMENSIONS (NON-TUNABLE CORE LINE DESIGNED ACCORDING TO QUARTER-WAVE TRANSFORMATION)

Design	Length sizes decomposition (**$L_{sum}=L_1+2\times L_2$**)		
	Tunable core line part (L_1)	***Non-tunable core line parts (L_2)***	***Total length (L_{sum})***
1	4.5 cm	7.5 mm	6 cm
2	2.5 cm	7.5 mm	4 cm

III. ELECTROMAGNETIC CHARACTERIZATION RESULTS

Results of extensive characterizations of the S-parameters and field intensities are presented for both designs (with connectors integrated for real-world deployment).

A. Results for Design 1: LC-Filled Symmetric CPW

The surface current density J_{surf} (in mA/m) is quantified in Figure 7 for multiple viewing angles, including a zoomed-in view of the coaxial mode at the connector pin section.

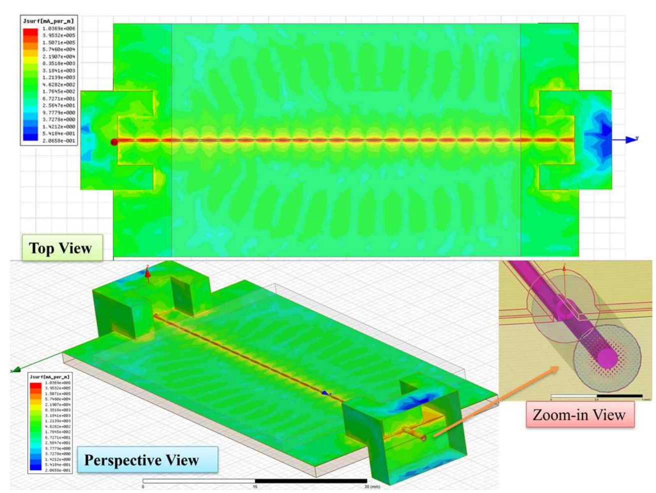

Figure 7. Surface current density visualized from multiple viewing angles, including a zoomed-in view of the coaxial mode at the connector pin.

S-parameters, including the forward transmission coefficient (S_{21}) and the forward reflection coefficient (S_{11}), recorded at LC biasing states of 0 V, 6 V, and 10 V, are presented jointly in Figure 8, alongside the derived maximally achievable differential phase shifts (recorded at the 6 V and 10 V biasing states). As denoted in Figure 8(c), the 0 V bias state of the LC is selected as the reference state for obtaining the differential phase shift at other biasing voltages (e.g., the intermediate bias of 6 V and the saturated bias of 10 V).

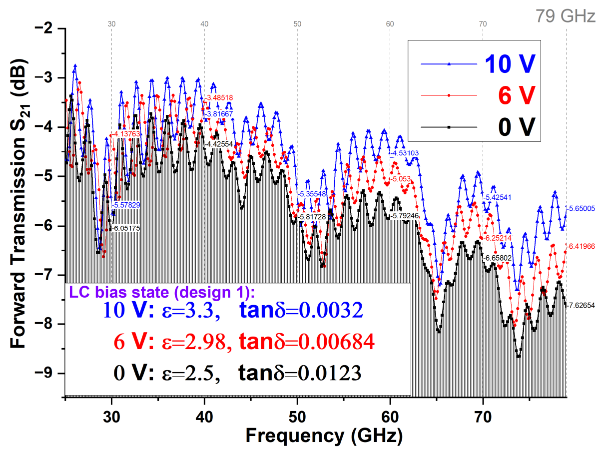

(a)

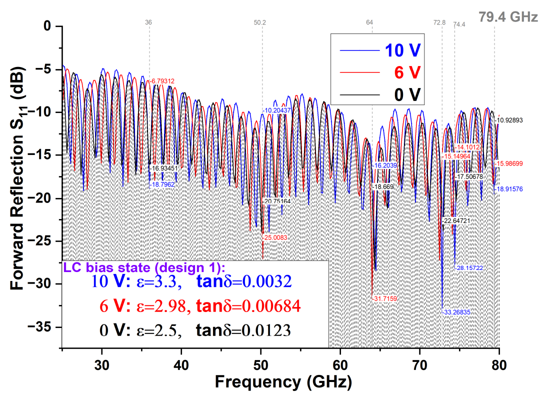

(b)

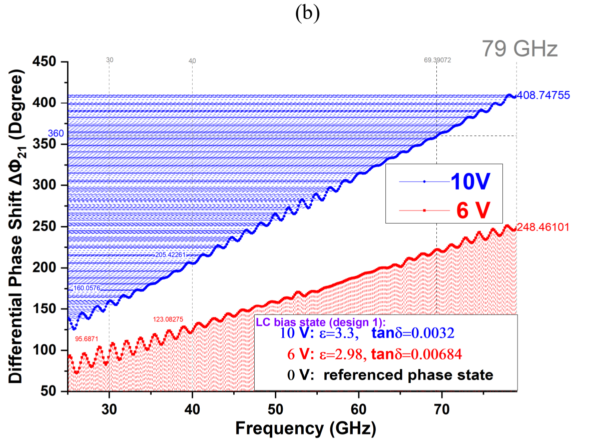

(c)

Figure 8. Characterized S-parameters of Design 1: (a) forward transmission coefficient (dB); (b) forward reflection coefficient (dB); (c) Differential phase shift at 6 V and 10 V biasing states of LC.

To comprehensively evaluate the ratio of the maximum differential phase shift to the maximum insertion loss (i.e., the minimum forward transmission), the universal figure-of-merit (FoM, expressed in °/dB) is defined and quantified in Figure 9. At 79 GHz, the maximum insertion loss for Design 1 is measured as 7.62654 dB at the 0 V LC bias state (Figure 8(a)), while the maximally achievable differential phase shift reaches 408.74755° at the 10 V LC bias state (Figure 8(c)). Consequently, the FoM at 79 GHz is derived as 408.74755° / 7.62654 dB ≈ 53.59°/dB for Design 1 (LC-filled symmetric CPW with connectors integrated).

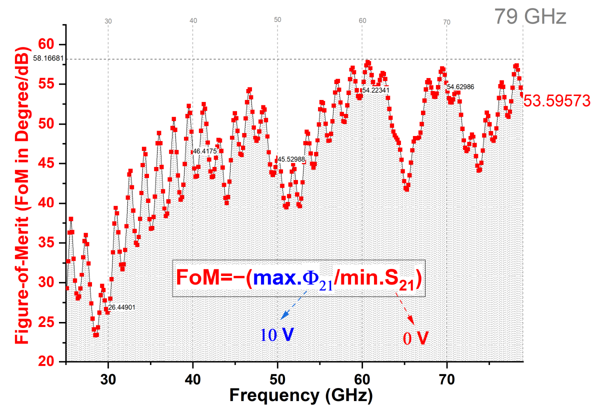

Figure 9. Derived FoM of Design 1 based on the maximally achievable differential phase shift (10 V bias state of LC) and maximum insertion loss (i.e., minimum forward transmission coefficient occurred at 0 V bias of LC).

B. Results for Design 2: Partially Shielded CPW Topology

Following the same computational characterization procedure employed for Design 1, the results for Design 2 are quantified below. Figure 10 presents the S-parameters, and Figure 11 depicts the corresponding FoM. As evidenced in Figure 11(a), the maximum insertion loss measures 9.64885 dB at the 0 V LC bias state. Notably, these results are not intended for direct comparison with those of Design 1, as the two designs differ in both the main line topology and the tunable line length (detailed in Table I), reflecting distinct phase shifting range functionalities. Specifically, Design 1 exhibits a maximum tuning range of up to 408.74755° (Figure 8), whereas Design 2 achieves a maximum tuning range of up to 347.79376° (Figure 10). The comprehensive evaluation yields an FoM of 38.19°/dB for Design 2, which employs a partially enclosed CPW topology for LC accommodation.

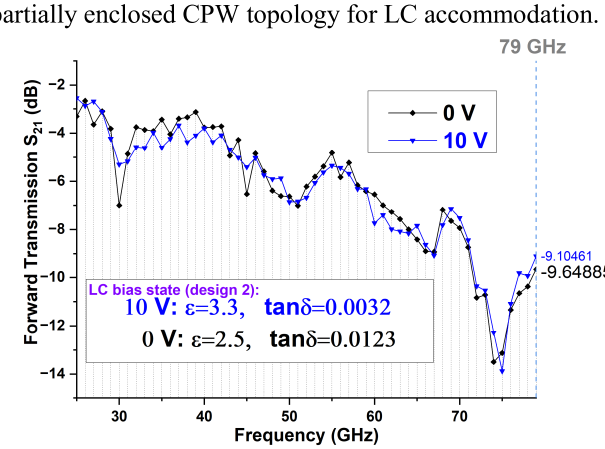

(a)

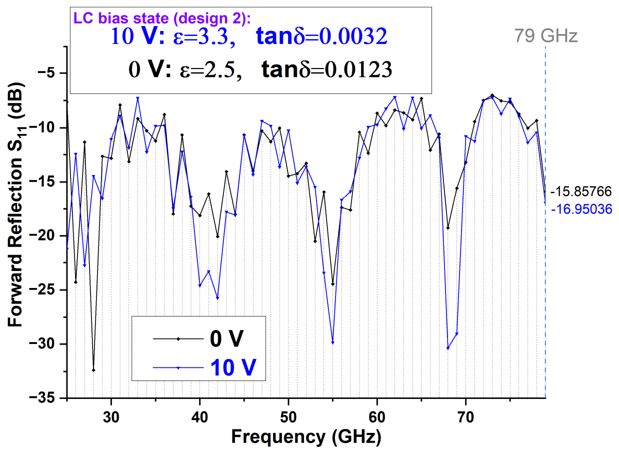

(b)

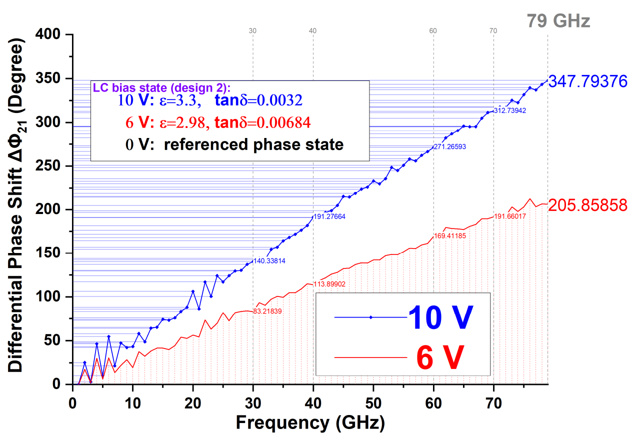

(c)

Figure 10. Characterized S-parameters of Design 2: (a) forward transmission coefficient (dB); (b) forward reflection coefficient (dB); (c) Differential phase shift at 6 V and 10 V biasing states of LC (taking 0 V bias state as the referenced phasing baseline).

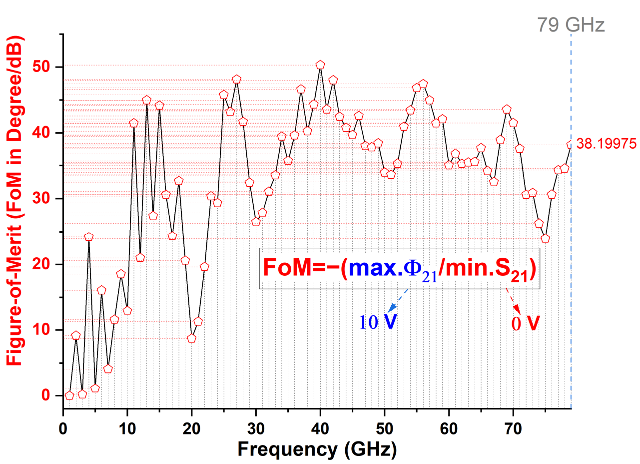

Figure 11. Derived FoM of Design 2 based on the ratio of the maximally achievable differential phase shift (occuring at the 10 V bias state of LC) and the maximum insertion loss (i.e., minimum forward transmission coefficient occurring at the 0 V bias state of LC).

IV. Conclusion and Outlook

This work has analytically and numerically investigated the electromagnetic effects of interface discontinuities in hybrid tunable/non-tunable PCB structures for 79 GHz liquid crystal (LC) phase shifters enabling joint communication and sensing (JC&S). Two legacy device topologies were examined: a symmetric coplanar waveguide (CPW) configuration with LC-filled coplanar gaps (Design 1), and a partially shielded CPW with integrated top electrodes and an additional LC tuning layer (Design 2). By deliberately maintaining non-tunable PCB sections as straight lines rather than optimized tapered shapes, and by incorporating 1.85 mm PCB-mount connectors, the study isolated and quantified the electromagnetic impacts arising from geometric and material discontinuities at the interfaces between tunable LC-filled core lines, non-tunable transition sections, and connector junctions.

Full-wave electromagnetic simulations using CST Studio Suite and ANSYS HFSS were conducted across the 1 GHz to 79 GHz frequency range. Quantitative analyses included S-parameters, surface current density distributions, maximally achievable differential phase shifts, and the figure-of-merit (FoM in °/dB). For Design 1 at 79 GHz, the maximum insertion loss was measured as 7.62654 dB at the 0 V LC bias state, while the maximally achievable differential phase shift reached 408.74755° at the 10 V bias state, yielding an FoM of approximately 53.59°/dB. For Design 2, the corresponding values were 9.64885 dB insertion loss at 0 V bias and a maximum phase shift of 347.79376°, resulting in an FoM of 38.19°/dB.

The results demonstrate that interface discontinuities—both between LC-filled core line segments and non-tunable counterparts, and between PCB edges and connector pins—induce higher-order mode propagation and impedance mismatches that significantly affect phase shifter performance at 79 GHz. The deliberate choice of non-optimized (straight-line) non-tunable sections revealed the extent to which material and geometric mismatches contribute to insertion loss and reduced FoM. Furthermore, the study assessed the viability of the classic quarter-wavelength transformation approach in multi-interface configurations, revealing that deviations from the standard 50 Ω impedance strategy—classically derived for coaxial lines as a trade-off between power handling and dissipation, which may not directly translate to planar PCB multi-interface configurations—may be necessary to accommodate these discontinuities.

Looking toward future JC&S deployments at 79 GHz, realizing multi-gigabit-per-second data links towards terabit-class aggregate throughput—potentially via spatial multiplexing in massive multiple-input multiple-output (MIMO) architectures or through coordinated multi-point (CoMP) operation—requires high-performance, low-loss beam-steering front-ends. The interface discontinuity effects quantified in this study directly impact insertion loss and phase accuracy, both of which are first-order determinants of link budget and beamforming precision. Mitigating these discontinuities through optimized transition geometries and improved connector integration strategies will therefore be essential to unlocking the full throughput potential of 79 GHz JC&S systems.

These findings illustrate the importance of rigorous electromagnetic characterization of interface regions in LC-based mmW phase shifters, particularly for emerging JC&S applications at 79 GHz that demand both high phase resolution and low loss (more specifically, low power consumption coupled with low insertion loss). Future work may focus on optimizing non-tunable section geometries (e.g., tapered transitions) and exploring advanced connector integration strategies to mitigate discontinuity-induced effects, thereby enhancing the overall performance of reconfigurable beam-steering systems for next-generation wireless platforms.

ACKNOWLEDGMENT

The author acknowledges the National Natural Science Foundation of China under Grant 62301043, and Beijing Institute of Technology Research Fund Program for Young Scholars. The author thanks University of Southampton and Imperial College London for offering the computational suite.

REFERENCES

[1] O. B. Akan, E. Dinc, M. Kuscu, O. Cetinkaya, and B. A. Bilgin, "Internet of Everything (IoE) - From Molecules to the Universe," *IEEE Commun. Mag.*, vol. 61, no. 10, pp. 122–128, October 2023.

[2] J. Li and H. Li, "Computationally Sampling Surface and Volume Current Densities of Liquid Crystal Non-Planar Phase Shifters for Low-Loss 5G IoT and 6G AIoT," in *Proc. 2024 IEEE International Conference on Omni-layer Intelligent Systems (IEEE COINS)*, London, United Kingdom, 2024, pp. 1–6.

[3] J. Li and H. Zhou, "Impact of Radial Grounding Model Granularity on Directivity of 433 MHz Monopole Antennas with Flat and Inclined Radials for ISM IoT Applications," *Ann. Emerg. Technol. Comput.*, vol. 9, no. 1, pp. 44–57, January 2025.

[4] J. Li and H. Li, "Liquid Crystal Technology for IoT and Beyond: Advancements and Future Directions," in *Proc. 2025 IEEE/IFAC International Conference on Control, Automation, and Instrumentation (IC2AI)*, Beirut, Lebanon, 2025, pp. 1–5.

[5] J. Li and H. Zhou, "Comparative Radiation Analysis of Vertical and Circular Disk Monopole Antennas for 433 MHz LoRa IoT Applications Using Method of Moments," in *Proc. IEEE 12th International Conference on Wireless Networks and Mobile Communications (WINCOM)*, Riyadh, Saudi Arabia, 2025, pp. 1–6.

[6] J. Li and H. Li, "Liquid Crystal-centric Artificial Intelligence of Things for Urban Scenes and City-scale Public Sector Modernization Towards General Reconfigurability for Artificial General Intelligence and Artificial Superintelligence," in *Proc. IEEE/IFAC 11th International Conference on Control, Decision and Information Technologies (CoDIT 2025)*, Split, Croatia, 2026, pp. 1684–1689.

[7] M. A. Fazlina, N. A. M. Yunus, N. N. Mohamed, M. M. Daud, and E. A. Sundararajan, "A Systematic Mapping: Exploring Internet of Everything Technologies and Innovations," *Symmetry*, vol. 15, no. 1, 1964, October 2023.

[8] V. V. Rostov, I. V. Romanchenko, A. V. Gunin, et al., "Review of Experiments on Microwave Beam Steering in Arrays of High-Power Oscillators by the Control of Voltage Rise Time," *IEEE Trans. Plasma Sci.*, vol. 46, no. 10, pp. 3640–3647, October 2018.

[9] F. Mehmood and A. Mehmood, "Recent Advancements in Millimeter-Wave Antennas and Arrays: From Compact Wearable Designs to Beam-Steering Technologies," *Electronics*, vol. 14, no. 13, 2705, July 2025.

[10] A. Wyner, "Recent results in the Shannon theory," *IEEE Trans. Inf. Theory*, vol. 20, no. 1, pp. 2–10, January 1974.

[11] J. Li, "79 GHz Meandering Enclosed-Coplanar Variable Delay Lines in Liquid Crystals Encapsulated Within Independent and Shared Cavities," in *Proc. IEEE 27th International Symposium on Antennas and Propagation (ISAP)*, Sydney, Australia, 2022, pp. 457–458.

[12] R. Thomä, T. Dallmann, S. Jovanoska, P. Knott, and A. Schmeink, "Joint Communication and Radar Sensing: An Overview," in *Proc. 2021 15th European Conference on Antennas and Propagation (EuCAP)*, Dusseldorf, Germany, 2021, pp. 1–5.

[13] J. Li and H. Li, "Passively Balanced Tunable Metasurface Feed for Analog Beamforming Free of Complex Digital Control Circuitry and Active Compensation," in *Proc. 2025 18th IEEE United Conference on Millimeter Waves and Terahertz Technologies (UCMMT)*, Nanjing, China, 2025, pp. 1–3.

[14] A. C. Patil, N. Rashmi, R. B. Vasishta, V. Charithra, and D. S. Bhat, "Integration of PIN Diodes for Beam Steering in Compact Microstrip Antenna Arrays," in *Proc. 2025 3rd International Conference on Integrated Circuits and Communication Systems (ICICACS)*, Raichur, India, 2025, pp. 1–8.

[15] J. Li and H. Li, "Effective Dielectric Constant Benchmark of 60 GHz Liquid Crystal-Filled Coaxial Delay Line," in *Proc. 2024 IEEE International Conference on Computational Electromagnetics (ICCEM)*, Nanjing, China, 2024, pp. 1–3.

[16] J. Li, "80 GHz Phase Shifter in Liquid Crystal Compact Coplanar Transmission Line with Curved Bends," in *Proc. IEEE 4th International Conference on Electrical, Computer and Energy Technologies (ICECET)*, Sydney, Australia, 2024, pp. 1–4.

[17] J. Li, "Challenges and Opportunities for Nematic Liquid Crystals in Radio Frequency and Beyond," *Crystals*, vol. 12, no. 5, 632, April 2022.

[18] J. Li, H. Xu, and D. Chu, "Design of liquid crystal based coplanar waveguide tunable phase shifter with no floating electrodes for 60–90 GHz applications," in *Proc. 2016 46th European Microwave Conference (EuMC)*, London, 2016, pp. 1047–1050.

[19] J. Li, "All-optically Controlled Microwave Analog Phase Shifter with Insertion Losses Balancing," *Engineering Letters*, vol. 28, no. 3, pp. 663–667, August 2020.

[20] J. Li and D. Chu, "Liquid crystal-based enclosed coplanar waveguide phase shifter for 54–66 GHz applications," *Crystals*, vol. 9, no. 12, 650, December 2019.

[21] J. Li, H. Li and Y. Xiao, "Unified Interpretation of Angular and Cumulative Angular Phase Representations with Best-Practice Guidelines for Differential Phase Shift Extraction in Nematic Liquid Crystal-Based Reconfigurable Phase Shifters," *Crystals*, vol. 15, no. 11, 994, November 2025.

[22] J. Li, "Roadmap of 6G Reconfigurable Intelligent Surfaces with Nematic Liquid Crystals: Fundamentals, State-of-the-Art, and Challenges," in *Proc. IEEE/IFAC 10th International Conference on Control, Decision and Information Technologies (CoDIT 2024)*, Vallette, Malta, 2024, pp. 802–807.

[23] J. Li, "Wideband PCB-to-Connectors Impedance Adapters for Liquid Crystal-Based Low-Loss Phase Shifters," in *Proc. 50th European Microwave Conference (EuMC)*, Utrecht, Netherlands, 2021, pp. 546–549.

[24] J. Li, "Towards Fabrication of High-tuning-range Liquid Crystals High-aspect-ratio Coplanar Waveguide Phase Shifter by LIGA, DRIE and Laser Ablation," in *Proc. 2023 Cross Strait Radio Science and Wireless Technology Conference*, Guilin, China, February 2024, pp. 1–3.

[25] J. Li, "Experimental Characterization of Patterned Electrodes and Shaped Substrates for A Liquid Crystals Phase Shifter at V Band," in *Proc. IEEE 15th International Conference on Microwave and Millimeter Wave Technology*, Qingdao, China, 2023, pp. 1–3.

[26] J. Li, "Millimetre-wave beam steering with analog-resolution and minimised distortion based on liquid crystals tunable delay lines with enhanced signal-to-noise ratios," *Proc. SPIE*, *Millimetre Wave and Terahertz Sensors and Technology XIII*, vol. 11541, 115410H, September 2020.

[27] J. M. Drozd and W. T. Joines, "Using parallel resonators to create improved maximally flat quarter-wavelength transformer impedance-matching networks," *IEEE Trans. Microw. Theory Tech.*, vol. 47, no. 2, pp. 132–141, February 1999.